

Enhanced Reverse Intersystem Crossing Promoted by Triplet Exciton–Photon Coupling

Qi Ou, Yihan Shao, and Zhigang Shuai*

Cite This: <https://doi.org/10.1021/jacs.1c08881>

Read Online

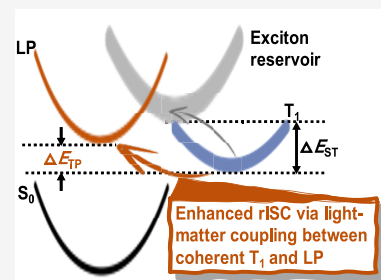
ACCESS |

Metrics & More

Article Recommendations

Supporting Information

ABSTRACT: Polaritons are hybrid light–matter states formed via strong coupling between excitons and photons inside a microcavity, leading to upper and lower polariton (LP) bands splitting from the exciton. The LP has been applied to reduce the energy barrier of the reverse intersystem crossing (rISC) process from T_1 , harvesting triplet energy for fluorescence through thermally activated delayed fluorescence. The spin–orbit coupling between T_1 and the excitonic part of the LP was considered as the origin for such an rISC transition. Here we propose a mechanism, namely, rISC promoted by the light–matter coupling (LMC) between T_1 and the photonic part of LP, which is originated from the ISC-induced transition dipole moment of T_1 . This mechanism was excluded in previous studies. Our calculations demonstrate that the experimentally observed enhancement to the rISC process of the erythrosine B molecule can be effectively promoted by the LMC between T_1 and a photon. The proposed mechanism would substantially broaden the scope of the molecular design toward highly efficient cavity-promoted light-emitting materials and immediately benefit the illumination of related experimental phenomena.



INTRODUCTION

In organic microcavities, molecular excitons may strongly couple to the quantized radiation field, forming hybridized light–matter states, which are known as exciton polaritons.^{1–5} Over the past few decades, exciton polaritons have been extensively investigated both experimentally and theoretically, offering a vast number of potential applications in the field of physical and chemical sciences such as manipulating chemical reactivities,^{6–9} promoting remote energy transfer,^{10–13} modifying the rate constants of electronic relaxation,^{7,14,15} and realizing polaritonic lasers.^{16–19} One of the interesting applications of exciton polaritons is the enhancement to the reverse intersystem crossing (rISC) process of thermally activated delayed fluorescence (TADF) materials, which could further increase the exciton utilization efficiency under current injection and thus would be strongly favored in organic light-emitting devices.^{20–23}

While multiple studies have reported the polariton-enhanced rISC process within organic molecules,^{15,24–26} whether such enhancement is indeed effective remains an open question. As pointed out by Yuen-Zhou and co-workers, at light–matter resonance, the rISC rate constant from a triplet to the polariton state is inversely proportional to the number of molecules coupling with the photon (denoted as N_{eff}), given that the polariton is delocalized across N_{eff} singlets and only one of them can undergo coupling to a given localized triplet.^{27,28} Therefore, organic microcavity systems, of which the number of coupled molecules can be as large as 10^5 to 10^6 , can hardly obtain an enhanced rISC process unless (i) the singlet–triplet mixing of the emitter is weak and (ii) the transition between triplet and singlet excitons is within the

inverted Marcus regime, as theoretically demonstrated via a quantum mechanical model in ref 27. A direct calculation of the experimentally observed polariton-enhanced rISC rate constant of realistic systems is, however, yet to be performed to essentially resolve the ambiguity. Accurate prediction on the rISC rate constant is a long-standing challenge for theoretical chemistry since it spans a wide time scale depending on the target systems and can be significantly longer than the typical time span of the best-available excited state dynamics simulation nowadays.^{29–31} Rate formalism such as the thermal vibration correlation function (TVCF) theory has become the practical approach to quantitatively describe the ISC/rISC process.^{32–34}

In this work, focusing on one of the reported systems with a polariton-enhanced rISC phenomenon, i.e., the erythrosine B (ErB) molecule (see Figure S1 for its chemical structure),¹⁵ we apply a properly benchmarked electronic structure theory and the TVCF rate formalism to quantify its rISC enhancement inside the cavity. Most importantly, while the spin–orbit coupling (SOC) between triplets and singlets and/or polaritons has been considered as the only promoting force for rISC, we propose that the light–matter coupling (LMC) between T_1 and the cavity mode can be another promoting

Received: August 23, 2021

force that initiates rISC inside the cavity for molecules with a non-negligible transition dipole moment (TDM) of T_1 such as ErB. The good agreement between our computational results and the previous experimental data rationalizes our theoretical protocol and demonstrates that the enhancement to the rISC of ErB inside the cavity can be effectively promoted by the LMC between T_1 and the photon. The proposed mechanism on the polariton-enhanced rISC process can be immediately applied to vindicate related experimental observations as well as enlighten the design of organic microcavities with efficient TADF phenomena.

THEORY

For N identical molecules that lie inside an optical cavity, in the strong coupling regime, the coupling strength of the i th molecule to the vacuum electromagnetic field is⁴

$$\hbar g_i = \|\boldsymbol{\mu}\| \sqrt{\frac{\hbar \omega_c}{2\epsilon_0 \epsilon_\infty V}} \cos \theta_i \quad (1)$$

where $\boldsymbol{\mu}$ is the TDM of the S_1 state; ω_c is the frequency of the cavity mode; ϵ_0 is the vacuum permittivity; ϵ_∞ is the optical dielectric constant of the matrix inside the cavity; V is the cavity mode volume; and θ_i is the angle between the TDM of the i th S_1 and the electromagnetic field. Note that if $\theta_i = 90^\circ$, the S_1 state of the i th molecule will not effectively couple to the field.

Supposing the excitonic coupling among the S_1 states of these N molecules is insignificant, we would have one lower polariton (LP) state and one upper polariton (UP) state, as well as $N - 1$ purely excitonic states.³⁵ If the cavity photon energy is resonant with the electronic transition, the energy difference between LP and UP at normal incidence is known as the Rabi splitting, which can be expressed as

$$\hbar \Omega_R = 2 \sqrt{\sum_i (\hbar g_i)^2} = 2 \|\boldsymbol{\mu}\| \sqrt{\frac{\hbar \omega_c \sum_{i=1}^N \cos^2 \theta_i}{2\epsilon_0 \epsilon_\infty V}} \quad (2)$$

If these N excitons are randomly oriented, the average value of $\cos^2 \theta_i$ is

$$\overline{\cos^2 \theta} = \frac{1}{4\pi} \int_0^\pi \cos^2 \theta \sin \theta \, d\theta \int_0^{2\pi} d\varphi = \frac{1}{3} \quad (3)$$

The Rabi splitting within such a random orientation model becomes

$$\hbar \Omega_R = \frac{2}{\sqrt{3}} \|\boldsymbol{\mu}\| \sqrt{\frac{\hbar \omega_c N}{2\epsilon_0 \epsilon_\infty V}} = \frac{2}{\sqrt{3}} \|\boldsymbol{\mu}\| \sqrt{\frac{\hbar \omega_c C}{2\epsilon_0 \epsilon_\infty}} \quad (4)$$

where C is the doping concentration of the light-emitting molecule in the matrix.

The LP state can be expressed as (following the Tavis–Cummings model)³

$$|\text{LP}\rangle = C_0 |g; 1\rangle + C_1 |e_1^S; 0\rangle + C_2 |e_2^S; 0\rangle + \dots + C_N |e_N^S; 0\rangle \quad (5)$$

Note that 0 and 1 denote the photon states; $|g; 1\rangle$ represents the state with all molecules in the ground state and a cavity photon; $|e_i^S; 0\rangle$ represents the state with the i th molecule being excited and the cavity mode is in its ground state. The normalization condition reads

$$C_0^2 + \sum_{i=1}^N C_i^2 = 1 \quad (6)$$

The energy of the LP is delocalized within N excitons and one cavity photon, and the value of C_0^2 represents the photon contribution of the LP. Practically, $\{C_i\}$ ($i = 0, \dots, N$) depends on the angle of incidence and the detuning value (the energy difference between the exciton absorption energy and the photon). For simplicity, we only consider the case at normal incidence.

Normally, the rISC process corresponds to the electronic transition from triplets to singlets promoted by SOC. According to Fermi's golden rule (FGR) and the TVCF rate formalism, the rISC rate constant can be calculated as^{20,36}

$$k_{\text{rISC}} = \frac{1}{\hbar^2} |H_{\text{if}}^{\text{SO}}|^2 \int_{-\infty}^{+\infty} dt e^{i\omega_{\text{if}} t} \rho_{\text{if}}(t, T) \quad (7)$$

where $H_{\text{if}}^{\text{SO}}$, ω_{if} and $\rho_{\text{if}}(t, T)$ correspond to the SOC constant, the frequency difference, and the Franck–Condon overlap between the initial (triplet) and final (singlet) state. Within a strong LMC regime, the rISC process may also take place between the triplet state and the LP state, of which the rate constant might be significantly altered. To compute the rISC rate constant from a triplet to an LP, one first needs to notice that vibronic decoupling will occur if the Rabi frequency is larger than the highest frequency vibrational modes coupled to the exciton states.^{28,37,38} In such a scenario, the geometric configuration of the LP remains the same as that of the ground state. Therefore, the Franck–Condon overlap that enters the FGR rate equation would become the one between the triplet and the ground state (instead of that between triplet and singlet excited states). As shown experimentally via the absorption and emission spectra in ref 15, such vibronic decoupling indeed takes place for ErB inside the cavity under strong LMC; that is, the absorption and emission peaks are identical. If one takes the vibronic decoupling effect into account and considers the SOC between T_1 and the excitonic part of the LP as the only promoting force, the rISC rate constant from triplet to LP (termed $k_{\text{rISC},1}^{\text{T}_1 \rightarrow \text{LP}}$ here) becomes

$$k_{\text{rISC},1}^{\text{T}_1 \rightarrow \text{LP}} = \frac{1}{\hbar^2} |H_{\text{if}}^{\text{SO}}|^2 \int_{-\infty}^{+\infty} dt e^{i[\omega_{\text{if}} - \frac{\Omega_R}{2}]t} \rho_{0T_1}(t, T) \times \frac{\sum_i C_i^2}{N_{\text{eff}}} \quad (8)$$

where $\rho_{0T_1}(t, T)$ is the Franck–Condon overlap between the ground state and the T_1 state and N_{eff} corresponds to the effective number of molecules that couple to the field. Note that under a random orientation assumption, N_{eff} is around one-third of the total molecule inside the cavity, as can be easily seen from eq 4. The classical limit of eq 8 is the Marcus equation for the rISC process from T_1 to LP triggered by SOC, which has been proposed and extensively discussed in refs 27 and 28, and the mechanism of such an SOC-triggered rISC process is schematically depicted in Figure 1(a).

While eq 8 can be used to evaluate the polariton-enhanced rISC rate for most fluorescent molecules, what has been excluded is the transition from triplet to LP triggered by the coupling between the triplet state and the photonic part of the LP, i.e., the coupling to the first term of eq 5 from the triplet state. For molecules with a phosphorescent phenomenon or non-negligible TDM of T_1 , such coupling needs to be taken into consideration. If the TDM of T_1 is $\boldsymbol{\mu}_{T_1}$, then the collective

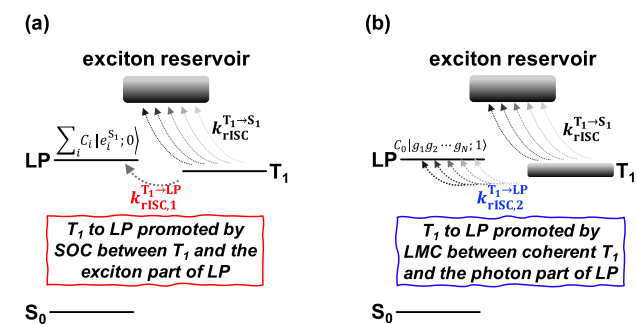


Figure 1. Schematic graph of two possible rISC channels. (a) T_1 to LP rISC process promoted by the SOC between T_1 and the exciton part of the LP, with the corresponding rate constant $k_{\text{rISC},1}^{T_1 \rightarrow \text{LP}}$. (b) T_1 to LP rISC process promoted by the collective LMC between coherent T_1 and the photonic part of the LP, with the corresponding rate constant $k_{\text{rISC},2}^{T_1 \rightarrow \text{LP}}$.

LMC between N randomly oriented triplet excitons and the cavity mode can be written as

$$\hbar\Omega_{T_1} = \frac{1}{\sqrt{3}} \|\mu_{T_1}\| \sqrt{\frac{\hbar\omega_c N}{2\epsilon_0\epsilon_\infty V}} = \frac{1}{\sqrt{3}} \|\mu_{T_1}\| \sqrt{\frac{\hbar\omega_c C}{2\epsilon_0\epsilon_\infty}} \quad (9)$$

where ω_c , C , ϵ_0 , and ϵ_∞ share the same definition as in eqs 2 and 4. Note that by coupling with the cavity mode, these triplets become coherent excitons and the collective LMC is enhanced by a factor of $\sqrt{N_{\text{eff}}}$ (compared with the case of molecular excited triplets),² which equals $\sqrt{N/3}$ with orientational average for randomly oriented excitons. A brief derivation of eq 9 is given in the Supporting Information. Owing to the fact that the TDM of the T_1 state is usually much smaller than that of a bright singlet state, even for phosphorescent molecules, the coupling strength between the triplet and the cavity mode is usually within the weak coupling regime; that is, *no hybrid polaritonic states will be formed between the triplet exciton and the photon*. For molecules with non-negligible TDM of T_1 , the rISC process triggered by the collective LMC between a set of coherent T_1 states and the cavity mode (termed $k_{\text{rISC},2}^{T_1 \rightarrow \text{LP}}$ here) can be expressed as

$$k_{\text{rISC},2}^{T_1 \rightarrow \text{LP}} = \frac{1}{\hbar^2} \left| \hbar\Omega_{T_1} \right|^2 \int_{-\infty}^{+\infty} dt e^{i(\omega_c - \frac{\Omega_B}{2})t} \rho_{0T_1}(t, T) \times C_0^2 \quad (10)$$

At resonance, $C_0^2 = \sum_i C_i^2 = 0.5$, $k_{\text{rISC},2}^{T_1 \rightarrow \text{LP}}$ would become significant if the TDM of T_1 is not negligible, and efficient rISC can then be initiated if the population on the triplet state after excitation is sufficient, which can be achieved via either a significantly faster ISC rate from S_1 to T_1 compared to the radiative/nonradiative decay rate of S_1/T_1 and the rISC rate from T_1 to S_1 under photoexcitation or the direct formation under current injection. The mechanism of the LMC-promoted rISC process from coherent T_1 to LP is schematically depicted in Figure 1(b).

RESULTS AND DISCUSSION

Outside the Cavity: Electronic Structure and Transitions of ErB. The geometries of the S_0 , S_1 , and T_1 states of isolated ErB molecules are first optimized via density functional theory (DFT) and time-dependent DFT (TDDFT) with the B3LYP functional and def2-svp basis set

with the corresponding def2 effective core potential (ECP). The excitation energies are then evaluated via spin-flip TDDFT (SF-TDDFT)^{39,40} with the B3LYP functional and def2-svp basis set with the corresponding ECP, since TDDFT gives severely deviant predictions of the absorption energy of S_1 and the emission energy of T_1 as shown in Table S1. It can be seen in Table 1 that the excitation energies computed via

Table 1. Absorption/Emission Energies of S_1 and T_1 , the 0–0 Singlet–Triplet Energy Gap $\Delta E_{\text{ST}}^{00}$, and Various Rate Constants of ErB Predicted by SF-TDDFT/B3LYP/def2-svp (with Corresponding ECP) and TVCF Rate Formalism^a

energetics	exptl (eV) ^b	calcd (eV)
S_1 absorption	2.305	2.448
S_1 emission	2.234	2.145
T_1 emission	1.845	1.893
$\Delta E_{\text{ST}}^{00}$	0.426	0.386
rate constants ^c	exptl (s ⁻¹) ^d	calcd (s ⁻¹)
k_F	2.8×10^8	1.5×10^8
k_{nr,S_1}	1.6×10^8	0.76×10^8
k_{ISC}	1.1×10^9	0.88×10^9
k_{rISC}	5.1×10^1	7.1×10^1
k_p	4.1×10^1	9.3×10^1
k_{nr,T_1}	1.5×10^3	1.3×10^3

^aExperimental results are also listed for comparison. ^bExperimental energetics are obtained from ref 15. ^c k_F , k_{nr,S_1} , k_{ISC} , k_{rISC} , k_p , and k_{nr,T_1} correspond to the fluorescent radiative decay rate of S_1 , the nonradiative decay rate from S_1 to S_0 , the ISC rate from S_1 to T_1 , the rISC rate from T_1 to S_1 , the phosphorescent radiative decay rate of T_1 , and the nonradiative decay rate from T_1 to S_0 , respectively. ^dExperimental rate constants are obtained from ref 42.

SF-TDDFT/B3LYP are in line with the experimental values. Two suggested functionals from a previous study, B5050LYP and PBES0,⁴¹ are tested for SF-TDDFT calculations, and the resultant energies are not as satisfying as those from B3LYP (as shown in Table S1). Explicit values of the TDM of S_1/T_1 and the SOC between S_0/S_1 and T_1 for ErB, as well as the computational details, are given in Methods and the Supporting Information.

With the electronic structure information, we calculate the rate constants of various electronic transitions via the TVCF rate formalism. Calculated results are listed in Table 1, together with the corresponding experimental values for comparison. An excellent agreement can be found between the theoretical predicted rate constants and their experimental counterparts, which rationalizes our applied electronic structure methods and the TVCF rate formalism. Note that the ISC rate constant of ErB is significantly larger than the radiative/nonradiative decay rate of S_1 and T_1 as well as the rISC rate, which leads to a sufficient population on the T_1 state after excitation and can thus contribute to the presumable enhancement of the rISC process inside the cavity.

Inside the Cavity: Light–Matter Coupling and Enhanced rISC. The next step is to calculate the LMC of ErB and the cavity mode at different doping concentrations (within the strong coupling regime) based on the experiments,¹⁵ 0.27, 0.36, 0.45, 0.54, and 0.61 M. It should be noted that ErB is a phosphorescent molecule with non-negligible TDM of T_1 . Therefore, we compute the Rabi splitting (which

stems from the LMC between S_1 and the photon) and the LMC strength between T_1 excitons and the cavity mode via eq 4 and eq 9, respectively. The optical dielectric constant ϵ_∞ of PVA is calculated as the square of its refractive index $n = 1.53$, i.e., $\epsilon_\infty = n^2 = 2.34$.^{43,44} It can be seen from Table 2 that the

Table 2. Rabi splitting and LMC between the T_1 Exciton of ErB and the Cavity Mode, as well as the Corresponding Excitation Energy of the LP and 0–0 LP–Triplet Energy Gap at Different Doping Concentrations

C (M)	$\hbar\Omega_R$ (eV)	$\hbar\Omega_{T_1}$ (cm ⁻¹)	E_{LP} (eV) ^a	$\Delta E_{LP,T_1}^{00}$ (eV)
0.27	0.292	1.184	2.302 (2.223)	0.339
0.36	0.338	1.367	2.279 (2.214)	0.316
0.45	0.377	1.528	2.259 (2.194)	0.301
0.54	0.413	1.674	2.241 (2.187)	0.283
0.61	0.439	1.780	2.228	0.270

^aIn the parentheses are experimental data obtained from ref 15 (which correspond to the emission energies of the LP at various doping concentrations).

Rabi splitting led by the coupling between S_1 and the cavity mode is large enough for all investigated doping concentrations, and two polaritonic bands can therefore be formed inside the cavity, which is consistent with the experimental absorption spectra. Specifically, when C is 0.54 M, the computed Rabi splitting is 413 meV and the corresponding excitation energy of the LP is 2.241 eV, which are in good agreement with the experimentally measured values (375 meV and 2.187 eV).¹⁵ The coupling from T_1 to the cavity mode is much smaller compared to that from S_1 , and therefore T_1 is unlikely to be hybridized with the photonic component for all doping concentrations, which is again consistent with the experimental findings that the phosphorescence spectra of the system basically remain the same with or without the cavity.¹⁵ However, such coupling may become the additional promoting force (other than SOC) that triggers the rISC process from T_1 to LP.

While it is nontrivial to evaluate the exact number of excitons that couple to the cavity mode due to the lack of some experimental details such as the cavity photon density, we assume the width and length of the cavity is two times the value of the experimentally measured thickness of the doped film, i.e., 130 nm, and evaluate the total number of emitters inside the cavity via

$$N = CVN_A \quad (11)$$

where N_A is the Avogadro constant. For $C = 0.54$ M, N is 2.8×10^6 based on eq 11, and the number of effectively coupled excitons N_{eff} is around 10^5 to 10^6 for randomly oriented molecules, which is of similar order as estimated in ref 28. If $N_{\text{eff}} = 10^5$ (at $C = 0.54$ M), the resulting $k_{\text{rISC},1}^{T_1 \rightarrow LP}$ evaluated from eq 8 will be less than 1 s^{-1} with a resonant condition as applied in the experiment ($\sum_i C_i^2 = C_0^2 = 0.5$). The experimentally observed enhancement of the T_1 decay rate is on the order of 10^3 ,¹⁵ which is significantly larger than the estimated value of $k_{\text{rISC},1}^{T_1 \rightarrow LP}$; that is, the enhancement of rISC of ErB inside the cavity cannot be rationally described via eq 8.

We now evaluate the enhanced rISC process from the other promoting force, i.e., the collective LMC between coherent T_1

and the cavity mode, and such an enhancement corresponds to $k_{\text{rISC},2}^{T_1 \rightarrow LP}$, which can be directly calculated via the TVCF rate formalism (as shown in eq 10) with the LMC given by eq 9. According to ref 15, the experimental rISC rate constant can be obtained by taking the reciprocal of the T_1 lifetime and subtracting the radiative and nonradiative decay rate constants of T_1 back to S_0 , namely, k_p and k_{nr,T_1} . Nevertheless, special attention needs to be paid here, as the decay processes of T_1 might be influenced by some nontrivial aggregation-induced effect when the doping concentration increases, which is irrelevant to the cavity-enhanced rISC. To make a reasonable comparison with the experimental data and rule out such an aggregation-induced effect, we define the experimental cavity-promoted enhancement of the rISC rate constant as the difference between the total decay rate of T_1 inside the cavity and that outside the cavity. Both the theoretical $k_{\text{rISC},2}^{T_1 \rightarrow LP}$ and the experimental enhancement are plotted in Figure 2 with respect

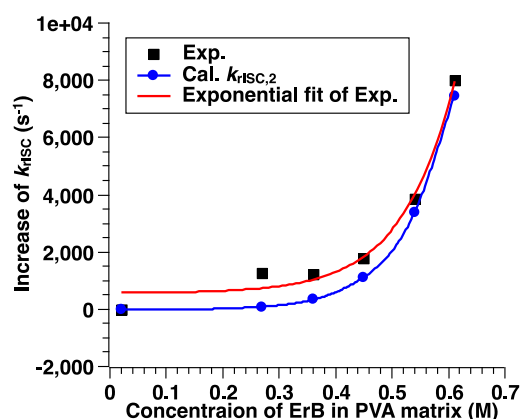


Figure 2. Experimental (black square) and calculated (blue circle) polaritonic enhancement to the rISC process of ErB with respect to different doping concentrations. The red line corresponds to an exponential fit based on the experimental data from ref 15.

to various doping concentrations. Explicit values of theoretical $k_{\text{rISC},2}^{T_1 \rightarrow LP}$ and experimental enhanced rISC rate for different doping concentrations are listed in Table S3. It can be seen from Figure 2 that the theoretically predicted enhancement given by eq 10 is in a good agreement with the experimentally observed enhancement for all tested doping concentrations, which evinces the fact that the LMC between T_1 and the cavity mode does act as an alternative promoting force and enhances the rISC process. With the increase of the doping concentration, the energy barrier of the rISC process is decreased and the coupling between T_1 and the cavity mode is increased, leading to a continuously enhanced rISC from T_1 to LP. We also investigate the individual effect of the reduced energy barrier and the increased LMC between T_1 and the field to the overall enhancement of the rISC process inside the cavity, as shown in Figure S2. Note that even though the total enhancement of $k_{\text{rISC},2}^{T_1 \rightarrow LP}$ mainly stems from the reduced energy barrier as the doping concentration increases, the LMC between T_1 and LP is the essential precondition that initiates such an rISC process.

Next, we consider the temperature effects on the enhanced rISC process. The rISC process of ErB is a thermally activated process and thus is very sensitive to the change of temperature. Experimentally, the increase of rISC rate constant with respect

to the increase of the temperature has been observed inside the cavity within a wide temperature range (from 283 to 333 K) for $C = 0.54$ M. Theoretically, we calculate $k_{\text{rISC},2}^{\text{T}_1 \rightarrow \text{LP}}$ at different temperatures with the rISC energy barrier and coupling strength obtained from $C = 0.54$ M, and the results are shown in Figure 3, together with the experimentally observed rISC

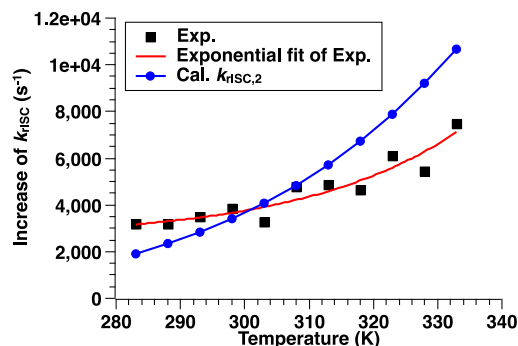


Figure 3. Experimental (black squares) and calculated (blue circles) polaritonic enhancement to the rISC process of ErB with respect to different temperatures. The red line corresponds to an exponential fit based on the experimental enhancement computed via the data from ref 15.

enhancement at different temperatures for comparison. Explicit values are listed in Table S4. As shown in Figure 3, the theoretically predicted enhancement of the rISC process qualitatively matches with the experimental results within the tested temperature range. A more rapid growth with respect to the temperature is found in the theoretical results, which may correspond to a slightly overestimated energy barrier according to the Arrhenius law. Such a discrepancy may also arise from the fact that the optical dielectric constant of PVA marginally changes as the temperature increases. The overall tendency of the rISC enhancement inside the cavity, however, can be qualitatively reproduced via the theoretically computed $k_{\text{rISC},2}^{\text{T}_1 \rightarrow \text{LP}}$, and this agreement further justifies the rationality of the LMC between T_1 and the cavity mode acting as an effective promoting force that enhances the rISC process for ErB. The temperature dependence of $k_{\text{rISC},1}^{\text{T}_1 \rightarrow \text{LP}}$ has also been investigated in Figure S3. As shown in Figure S3, despite the fact that $k_{\text{rISC},1}^{\text{T}_1 \rightarrow \text{LP}}$ given by eq 8 has a remarkable temperature dependence, its contribution to the overall enhancement would still be negligible even at high temperatures, due to the large number of molecules that effectively couple to the cavity.

As we have shown above, by taking the collective LMC between T_1 and the cavity mode into account, we are able to reproduce the experimentally observed enhancement to the rISC rate of ErB inside the cavity via the TVCF rate formalism. Note that this enhanced rISC channel might be safely ignored for fluorescent molecules with a negligible TDM of T_1 . For example, the molecule that has been investigated in ref 28, 3DPA3CN, is a TADF molecule with almost no phosphorescence even at low temperature,⁴⁵ which corresponds to an infinitesimal LMC between T_1 and the cavity mode. Therefore, the rISC of 3DPA3CN inside the cavity is not noticeably enhanced via $k_{\text{rISC},2}^{\text{T}_1 \rightarrow \text{LP}}$. In addition to the TDM of T_1 , another key factor to obtain considerable enhancement of the rISC via the LMC between T_1 and the field is that T_1 possesses a substantial population after the excitation, which may be

introduced via either the direct formation of triplets under current injection or a significantly faster ISC rate compared to the radiative and nonradiative decay rate of S_1 and T_1 under photoexcitation. It should be noted that even though the tested system here (ErB) is a phosphorescent molecule, such enhancement via $k_{\text{rISC},2}^{\text{T}_1 \rightarrow \text{LP}}$ can be expected for normal TADF emitters as long as the T_1 state of these emitters has a sizable ISC-induced TDM.

CONCLUSION

In summary, we have unravelled an alternative promoting force, in addition to the SOC between T_1 and LP, for the polariton-enhanced rISC process inside the cavity, i.e., the collective LMC between coherent T_1 states and the cavity mode that initiates the conversion from T_1 to LP without perturbing the energy level of the original T_1 state. This promoting force is necessary to be taken into account for molecules with a non-negligible TDM of T_1 . With this revised mechanism, we are able to reproduce the experimentally observed polariton-enhanced rISC rate constant of ErB inside a cavity and demonstrate that the enhanced rISC of ErB inside the cavity can be effectively promoted by the LMC between its T_1 and the cavity mode. While the effect of the LMC between T_1 and the LP on the rISC process has rarely been investigated in previous studies, what we have concluded here is that such coupling makes it possible for poor or even non-TADF emitters to harvest a triplet exciton for fluorescence inside a cavity, as long as these emitters have a sizable TDM of T_1 . Such findings will substantially widen the scope of TADF candidates. Looking forward, we believe this theoretical protocol would immediately benefit the illumination of important experimental phenomena as well as the design of polariton-enhanced TADF systems.

METHODS

All of the electronic structure calculations are carried out using quantum chemistry package Q-CHEM 5.3⁴⁶ except for the TDM calculation of T_1 , which is performed using DALTON.⁴⁷ All of the rate constant calculations are performed in our self-developed molecular material property prediction package MOMAP 2021A.^{48–50} The SOC constants between singlet and triplet (constructed from TDDFT/B3LYP) of ErB are evaluated in a local developed version of Q-CHEM via the Breit–Pauli Hamiltonian⁵¹ (one-electron part only) with the effective nuclear charge (ENC) obtained from ref 52 for C, H, O, and Na and from ref 53 for I. All elements are tackled with the all-electron basis set for the calculation of SOC and the TDM of T_1 , i.e., 6-311G** for I and def2-svpd for C, H, O, and Na, and the values of ENC obtained from the literature correspond to those used for the all-electron basis set. The TDM of S_1 is calculated via SF-TDDFT/B3LYP/def2-svpd (with corresponding def2 ECP), while that of T_1 is calculated via the quadratic response method.⁵⁴ Additional computational details can be found in the Supporting Information.

ASSOCIATED CONTENT

Supporting Information

The Supporting Information is available free of charge at <https://pubs.acs.org/doi/10.1021/jacs.1c08881>.

Excitation energies of S_1 and T_1 of ErB predicted by TDDFT/B3LYP/def2-svpd and SF-TDDFT/PBES0-(B5050LYP)/def2-svpd; TDM of S_1 and T_1 of ErB, SOC between S_0/S_1 and T_1 of ErB, explicit rate constants of theoretically predicted $k_{\text{rISC},2}^{\text{T}_1 \rightarrow \text{LP}}$ and exper-

imentally observed rISC enhancement, the individual effect of the reduced energy barrier and the increased LMC strength on the overall $k_{\text{rISC},2}^{\text{T}_1 \rightarrow \text{LP}}$, temperature dependence of estimated $k_{\text{rISC},1}^{\text{T}_1 \rightarrow \text{LP}}$ for $C = 0.54 \text{ M}$, and additional computational details (PDF)

AUTHOR INFORMATION

Corresponding Author

Zhigang Shuai – MOE Key Laboratory of Organic Optoelectronics and Molecular Engineering, Department of Chemistry, Tsinghua University, Beijing 100084, China; orcid.org/0000-0003-3867-2331; Email: zgshuai@tsinghua.edu.cn

Authors

Qi Ou – MOE Key Laboratory of Organic Optoelectronics and Molecular Engineering, Department of Chemistry, Tsinghua University, Beijing 100084, China; orcid.org/0000-0002-6400-7522

Yihan Shao – Department of Chemistry and Biochemistry, University of Oklahoma, Norman, Oklahoma 73019, United States; orcid.org/0000-0001-9337-341X

Complete contact information is available at:

<https://pubs.acs.org/10.1021/jacs.1c08881>

Notes

The authors declare no competing financial interest.

ACKNOWLEDGMENTS

Q.O. thanks Dr. Wenjie Dou and Dr. Jiajun Ren for helpful discussions on the light–matter coupling between a triplet and the cavity mode. Z.S. acknowledges financial support from the National Natural Science Foundation of China (Grant No. 21788102) as well as the Ministry of Science and Technology of China through the National Key R&D Plan (Grant No. 2017YFA0204501). Y.S. is supported by the National Science Foundation (Grant No. CHE-2102071). Q.O. acknowledges financial support from the National Natural Science Foundation of China (Grant No. 22003030), China Postdoctoral Science Foundation (Grant No. 2020M670280), and the Shuimu Tsinghua Scholar Program.

REFERENCES

- (1) Keeling, J.; Kéna-Cohen, S. Bose–Einstein Condensation of Exciton-Polaritons in Organic Microcavities. *Annu. Rev. Phys. Chem.* **2020**, *71*, 435–459.
- (2) Hertzog, M.; Wang, M.; Mony, J.; Börjesson, K. Strong Light–Matter Interactions: A New Direction within Chemistry. *Chem. Soc. Rev.* **2019**, *48*, 937–961.
- (3) Ribeiro, R. F.; Martínez-Martínez, L. A.; Du, M.; Campos-Gonzalez-Angulo, J.; Yuen-Zhou, J. Polariton Chemistry: Controlling Molecular Dynamics with Optical Cavities. *Chem. Sci.* **2018**, *9*, 6325–6339.
- (4) Ebbesen, T. W. Hybrid Light–Matter States in a Molecular and Material Science Perspective. *Acc. Chem. Res.* **2016**, *49*, 2403–2412.
- (5) Dovzhenko, D. S.; Ryabchuk, S. V.; Rakovich, Y. P.; Nabiev, I. R. Light–Matter Interaction in the Strong Coupling Regime: Configurations, Conditions, and Applications. *Nanoscale* **2018**, *10*, 3589–3605.
- (6) Schwartz, T.; Hutchison, J. A.; Genet, C.; Ebbesen, T. W. Reversible Switching of Ultrastrong Light-Molecule Coupling. *Phys. Rev. Lett.* **2011**, *106*, 196405.
- (7) Hutchison, J. A.; Schwartz, T.; Genet, C.; Devaux, E.; Ebbesen, T. W. Modifying Chemical Landscapes by Coupling to Vacuum Fields. *Angew. Chem., Int. Ed.* **2012**, *51*, 1592–1596.
- (8) Galego, J.; Garcia-Vidal, F. J.; Feist, J. Many-Molecule Reaction Triggered by a Single Photon in Polaritonic Chemistry. *Phys. Rev. Lett.* **2017**, *119*, 136001.
- (9) Munkhbat, B.; Wersäll, M.; Baranov, D. G.; Antosiewicz, T. J.; Shegai, T. Suppression of Photo-Oxidation of Organic Chromophores by Strong Coupling to Plasmonic Nanoantennas. *Sci. Adv.* **2018**, *4*, No. eaas9552.
- (10) Coles, D. M.; Niccolo Somaschi, P. M.; Clark, C.; Lagoudakis, P. G.; Savvidis, P. G.; Lidzey, D. G. Polariton-Mediated Energy Transfer between Organic Dyes in a Strongly Coupled Optical Microcavity. *Nat. Mater.* **2014**, *13*, 712–719.
- (11) Zhong, X.; Chervy, T.; Wang, S.; George, J.; Thomas, A.; Hutchison, J. A.; Devaux, E.; Genet, C.; Ebbesen, T. W. Non-Radiative Energy Transfer Mediated by Hybrid Light-Matter States. *Angew. Chem., Int. Ed.* **2016**, *55*, 6202–6206.
- (12) Zhong, X.; Chervy, T.; Zhang, L.; Thomas, A.; George, J.; Genet, C.; Hutchison, J. A.; Ebbesen, T. W. Energy Transfer between Spatially Separated Entangled Molecules. *Angew. Chem., Int. Ed.* **2017**, *56*, 9034–9038.
- (13) Georgiou, K.; Michetti, P.; Gai, L.; Cavazzini, M.; Shen, Z.; Lidzey, D. G. Control over Energy Transfer between Fluorescent BODIPY Dyes in a Strongly Coupled Microcavity. *ACS Photonics* **2018**, *5*, 258–266.
- (14) Kéna-Cohen, S.; Forrest, S. R. Green Polariton Photoluminescence Using the Red-Emitting Phosphor PtOEP. *Phys. Rev. B: Condens. Matter Mater. Phys.* **2007**, *76*, 075202.
- (15) Stranius, K.; Hertzog, M.; Börjesson, K. Selective Manipulation of Electronically Excited States through Strong Light–Matter Interactions. *Nat. Commun.* **2018**, *9*, 2273.
- (16) Kéna-Cohen, S.; Forrest, S. R. Room-temperature polariton lasing in an organic single-crystal microcavity. *Nat. Photonics* **2010**, *4*, 371–375.
- (17) Bittner, E. R.; Silva, C. Estimating the Conditions for Polariton Condensation in Organic Thin-Film Microcavities. *J. Chem. Phys.* **2012**, *136*, 034510.
- (18) Daskalakis, K. S.; Maier, S. A.; Murray, R.; Kéna-Cohen, S. Nonlinear Interactions in An Organic Polariton Condensate. *Nat. Mater.* **2014**, *13*, 271–278.
- (19) Paschos, G. G.; Somaschi, N.; Tsintzos, S. I.; Coles, D.; Bricks, J. L.; Hatzopoulos, Z.; Lidzey, D. G.; Lagoudakis, P. G.; Savvidis, P. G. Hybrid Organic-Inorganic Polariton Laser. *Sci. Rep.* **2017**, *7*, 11377.
- (20) Peng, Q.; Fan, D.; Duan, R.; Yi, Y.; Niu, Y.; Wang, D.; Shuai, Z. Theoretical Study of Conversion and Decay Processes of Excited Triplet and Singlet States in a Thermally Activated Delayed Fluorescence Molecule. *J. Phys. Chem. C* **2017**, *121*, 13448–13456.
- (21) Xu, S.; Yang, Q.; Wan, Y.; Chen, R.; Wang, S.; Si, Y.; Yang, B.; Liu, D.; Zheng, C.; Huang, W. Predicting Intersystem Crossing Efficiencies of Organic Molecules for Efficient Thermally Activated Delayed Fluorescence. *J. Mater. Chem. C* **2019**, *7*, 9523–9530.
- (22) Cui, L.-S.; Gillett, A. J.; Zhang, S.-F.; Ye, H.; Liu, Y.; Chen, X.-K.; Lin, Z.-S.; Evans, E. W.; Myers, W. K.; Ronson, T. K.; Nakanotani, H.; Reineke, S.; Bredas, J.-L.; Adachi, C.; Friend, R. H. Fast Spin-Flip Enables Efficient and Stable Organic Electroluminescence from Charge-Transfer States. *Nat. Photonics* **2020**, *14*, 636–642.
- (23) Zhan, X.; Wu, Z.; Gong, Y.; Tu, J.; Xie, Y.; Peng, Q.; Ma, D.; Li, Q.; Li, Z. Utilizing Electropole Emission to Achieve External Quantum Efficiency up to 18.1% in Nondoped Blue OLED. *Research* **2020**, *2020*, 8649102.
- (24) Xu, J.; Tang, X.; Zhao, X.; Zhu, H.; Qu, F.; Xiong, Z. Abnormal Reverse Intersystem Crossing of Polaron-Pair States and Its Conversion to Intersystem Crossing via the Regulation of Intermolecular Electron-Hole Spacing Distance. *Phys. Rev. Appl.* **2020**, *14*, 024011.

- (25) Polak, D.; et al. Manipulating Molecules with Strong Coupling: Harvesting Triplet Excitons in Organic Exciton Microcavities. *Chem. Sci.* **2020**, *11*, 343–354.
- (26) Yu, Y.; Mallick, S.; Wang, M.; Börjesson, K. Barrier-Free Reverse-Intersystem Crossing in Organic Molecules by Strong Light-Matter Coupling. *Nat. Commun.* **2021**, *12*, 3255.
- (27) Martínez-Martínez, L. A.; Eizner, E.; Kéna-Cohen, S.; Yuen-Zhou, J. Triplet Harvesting in the Polaritonic Regime: A Variational Polaron Approach. *J. Chem. Phys.* **2019**, *151*, 054106.
- (28) Eizner, E.; Martínez-Martínez, L. A.; Yuen-Zhou, J.; Kéna-Cohen, S. Inverting Singlet and Triplet Excited States Using Strong Light-Matter Coupling. *Sci. Adv.* **2019**, *5*, No. eaax4482.
- (29) Koch, A.; Kinzel, D.; Dröge, F.; Gräfe, S.; Kupfer, S. Photochemistry and Electron Transfer Kinetics in a Photocatalyst Model Assessed by Marcus Theory and Quantum Dynamics. *J. Phys. Chem. C* **2017**, *121*, 16066–16078.
- (30) Menger, M. F. S. J.; Plasser, F.; Mennucci, B.; González, L. Surface Hopping within an Exciton Picture. An Electrostatic Embedding Scheme. *J. Chem. Theory Comput.* **2018**, *14*, 6139–6148.
- (31) Westermayr, J.; Gastegger, M.; Menger, M. F. S. J.; Mai, S.; González, L.; Marquetand, P. Machine Learning Enables Long Time Scale Molecular Photodynamics Simulations. *Chem. Sci.* **2019**, *10*, 8100–8107.
- (32) Shuai, Z.; Peng, Q. Excited States Structure and Processes: Understanding Organic Light-Emitting Diodes at the Molecular Level. *Phys. Rep.* **2014**, *537*, 123–156.
- (33) Wang, Y.; Peng, Q.; Ou, Q.; Lin, S.; Shuai, Z. A Novel Molecular Descriptor for Highly Efficient ($\Phi_{\text{TADF}} > 90\%$) Transition Metal TADF Au(III) Complexes. *J. Mater. Chem. A* **2020**, *8*, 18721–18725.
- (34) Lin, S.; Ou, Q.; Wang, Y.; Peng, Q.; Shuai, Z. Aggregation-Enhanced Thermally Activated Delayed Fluorescence Efficiency for Two-Coordinate Carbene–Metal–Amide Complexes: A QM/MM Study. *J. Phys. Chem. Lett.* **2021**, *12*, 2944–2953.
- (35) Houdré, R.; Stanley, R. P.; Ilegems, M. Vacuum-Field Rabi Splitting in the Presence of Inhomogeneous Broadening: Resolution of a Homogeneous Linewidth in an Inhomogeneously Broadened System. *Phys. Rev. A: At., Mol., Opt. Phys.* **1996**, *53*, 2711–2715.
- (36) Niu, Y.; Peng, Q.; Deng, C.; Gao, X.; Shuai, Z. Theory of Excited State Decays and Optical Spectra: Application to Polyatomic Molecules. *J. Phys. Chem. A* **2010**, *114*, 7817–7831.
- (37) Spano, F. C. Optical Microcavities Enhance the Exciton Coherence Length and Eliminate Vibronic Coupling in J-Aggregates. *J. Chem. Phys.* **2015**, *142*, 184707.
- (38) Herrera, F.; Spano, F. C. Cavity-Controlled Chemistry in Molecular Ensembles. *Phys. Rev. Lett.* **2016**, *116*, 238301.
- (39) Shao, Y.; Head-Gordon, M.; Krylov, A. I. The Spin–Flip Approach within Time-Dependent Density Functional Theory: Theory and Applications to Diradicals. *J. Chem. Phys.* **2003**, *118*, 4807–4818.
- (40) Bernard, Y. A.; Shao, Y.; Krylov, A. I. General Formulation of Spin-Flip Time-Dependent Density Functional Theory Using Non-Collinear Kernels: Theory, Implementation, and Benchmarks. *J. Chem. Phys.* **2012**, *136*, 204103.
- (41) Orms, N.; Krylov, A. I. Singlet–Triplet Energy Gaps and the Degree of Diradical Character in Binuclear Copper Molecular Magnets Characterized by Spin-Flip Density Functional Theory. *Phys. Chem. Chem. Phys.* **2018**, *20*, 13127–13144.
- (42) Lettinga, M. P.; Zuilhof, H.; van Zandvoort, M. A. M. J. Phosphorescence and Fluorescence Characterization of Fluorescein Derivatives Immobilized in Various Polymer Matrices. *Phys. Chem. Chem. Phys.* **2000**, *2*, 3697–3707.
- (43) Matsumoto, S.; Ishii, T.; Wada, M.; Kuwahara, Y.; Ogata, T.; Nagaoka, S.; Takafuji, M.; Ihara, H. Facile Preparation of High Refractive Index Polymer Films Compositing with a Tungstophosphoric Acid. *Mater. Lett.* **2017**, *190*, 236–239.
- (44) Robertson, J. In *Comprehensive Semiconductor Science and Technology*; Bhattacharya, P., Fornari, R., Kamimura, H., Eds.; Elsevier: Amsterdam, 2011; pp 132–176.
- (45) Taneda, M.; Shizu, K.; Tanaka, H.; Adachi, C. High Efficiency Thermally Activated Delayed Fluorescence Based on 1,3,5-tris(4-(diphenylamino)phenyl)-2,4,6-tricyanobenzene. *Chem. Commun.* **2015**, *51*, 5028–5031.
- (46) Shao, Y.; et al. Advances in Molecular Quantum Chemistry Contained in the Q-Chem 4 Program Package. *Mol. Phys.* **2015**, *113*, 184–215.
- (47) Aidas, K.; et al. The Dalton Quantum Chemistry Program System. *WIREs Comput. Mol. Sci.* **2014**, *4*, 269–284.
- (48) Shuai, Z.; Peng, Q. Organic Light-Emitting Diodes: Theoretical Understanding of Highly Efficient Materials and Development of Computational Methodology. *Nat. Sci. Rev.* **2017**, *4*, 224–239.
- (49) Peng, Q.; Yi, Y.; Shuai, Z.; Shao, J. Toward Quantitative Prediction of Molecular Fluorescence Quantum Efficiency: Role of Duschinsky Rotation. *J. Am. Chem. Soc.* **2007**, *129*, 9333–9339.
- (50) Shuai, Z. Thermal Vibration Correlation Function Formalism for Molecular Excited State Decay Rates. *Chin. J. Chem.* **2020**, *38*, 1223–1232.
- (51) Abegg, P. Ab Initio Calculation of Spin-Orbit Coupling Constants for Gaussian Lobe and Gaussian-Type Wave Functions. *Mol. Phys.* **1975**, *30*, 579–596.
- (52) Fedorov, D. G.; Koseki, S.; Schmidt, M. W.; Gordon, M. S. Spin-Orbit Coupling in Molecules: Chemistry beyond the Adiabatic Approximation. *Int. Rev. Phys. Chem.* **2003**, *22*, 551–592.
- (53) Chiodo, S. G.; Russo, N. One-Electron Spin-Orbit Contribution by Effective Nuclear Charges. *J. Comput. Chem.* **2009**, *30*, 832–839.
- (54) Vahtras, O.; Ågren, H.; Jørgensen, P.; Jensen, H. J. A.; Helgaker, T.; Olsen, J. Multiconfigurational Quadratic Response Functions for Singlet and Triplet Perturbations: The Phosphorescence Lifetime of Formaldehyde. *J. Chem. Phys.* **1992**, *97*, 9178–9187.